DALTON

Synthesis of sterically hindered bis(imidazole) proligands and an exploration of their co-ordination chemistry with copper(II)†

Timothy C. Higgs, Madeleine Helliwell and C. David Garner*

The Chemistry Department, University of Manchester, Oxford Road, Manchester M13 9PL, UK

Five new sterically hindered bis(imidazole) proligands have been synthesised: 1,2-bis(1-ethyl-4-phenylimidazol-2-yl)ethane (L^1), bis(1-ethyl-4-phenylimidazol-2-yl)-(L^2) and bis(1-methyl-4-phenylimidazol-2-yl)-dimethyl methane (L^3), α,α′-bis(4,5′-diphenylimidazol-1-yl)-*o*-(L^4) and *m*-xylene (L^5). They have been characterised analytically and spectroscopically (^{1}H NMR and mass) and L^1 and L^2 have been crystallised and characterised by X-ray crystallography. Complexation reactions were attempted with $Cu(BF_4)_2{\cdot}4.5H_2O$ but only L^1 formed a simple monomeric complex, $[CuL^1{}_2][BF_4]_2$. The Cu^{II} is co-ordinated by four nitrogen atoms, $Cu–N_{av}$ 2.01 Å, in an essentially square-planar environment. The X-band EPR spectrum of solid $[CuL^1{}_2][BF_4]_2$ ($g_\perp \approx 1.967$, $g_\parallel \approx 2.214$, $A_\parallel \approx 196 \times 10^{-4}$ cm^{-1}) is consistent with a tetragonal ligand field but the Q-band spectrum of a frozen solution of the complex in CH_2Cl_2–toluene (10:1) at 77 K indicates a small rhombic distortion ($g_x \approx 2.034$, $g_y \approx 2.052$ and $g_z \approx 2.229$, $A_z \approx 198 \times 10^{-4}$ cm^{-1}). In CH_2Cl_2 the complex displays a quasi-reversible Cu^{II}–Cu^{I} couple with an oxidation peak at +0.74 V and a coupled reduction at −0.07 V (scan rate of 0.2 V s^{-1}). The complexes $[CuL^4{}_2][BF_4]_2{\cdot}H_2O$ and $[CuL^5{}_2][BF_4]_2{\cdot}H_2O$ appear to be polymeric with bridging ligands. Compound L^3 reacted with $Cu(BF_4)_2{\cdot}4.5H_2O$ to form $[H_2L_3][BF_4]_2$ which has been characterised by X-ray crystallography; L^2 reacts similarly.

Imidazole is a ubiquitous ligand for copper in proteins, as the co-ordinating side-chain of the amino acid, histidine. The presence of imidazole ligation has been confirmed crystallographically in several proteins including plastocyanin,[1] azurin,[2] Cu–Zn superoxide dismutase,[3] haemocyanin,[4] galactose oxidase,[5] ascorbate oxidase,[6] and nitrite reductase.[7] The ubiquity of copper–imidazole bonding in copper metalloproteins has stimulated the synthesis and characterisation of many imidazoles and their copper complexes, in order to relate the spectroscopic properties of low-molecular-weight complexes to the natural systems. Most of these studies have involved monoimidazoles,[8–14] often with little or no specific modification. The use of these has several advantages, including ease of synthesis, but may be disadvantageous for several reasons. Copper(II) complexes of such compounds tend to be only soluble in co-ordinating solvents and studies of these solutions can be complicated by solvent-exchange effects. Thus, the EPR spectrum of $[Cu(1,4,5\text{-tmim})_4][ClO_4]_2$[12] (1,4,5-tmim = 1,4,5-trimethylimidazole) in MeOH at 298 K exhibits signals attributed to the presence of $[Cu(1,4,5\text{-tmim})_4]^{2+}$ and $[Cu(1,4,5\text{-tmim})_4(MeOH)]^{2+}$. Furthermore, monoimidazoles are prone to rotate freely in solution, leading to broader electronic spectra in solution than for the solid state, *e.g.* $[Cu(Him)_4(SO_4)]$ (Him = imidazole).[9] Such effects can mean that the properties of solutions of copper–imidazole complexes cannot be directly related to the crystal structure.

We have developed a programme of synthesis of sterically hindered imidazole proligands and an exploration of their co-ordination chemistry.[15–17] These confer the property of solubility in non-co-ordinating solvents (*e.g.* CH_2Cl_2) upon the resultant complexes, thus encouraging maintenance of the solid-state structure in solution. The use of bulky substituents should also result in complexes of paramagnetic metal centres being magnetically dilute, thereby enhancing the clarity of the solid-state EPR spectrum. Herein we report the synthesis and characterisation of some new, sterically hindered, bis(imidazoles) and an investigation of their co-ordination chemistry with copper(II).

† *Non-SI unit employed:* G = 10^{-4} T.

Experimental

Synthesis of proligands

***(a)* 1,2-Bis(1-ethyl-4-phenylimidazol-2-yl)ethane (L^1).** A four-step synthesis has been developed (see Scheme 1). The first three reactions, which lead to the formation of 1,2-bis-(4-phenylimidazol-2-yl)ethane, are based on the synthetic procedure developed by Schugar and co-workers[18] but with some slight modifications. An NH_4O_2CMe–HO_2CMe mixture was used in the third cyclisation step, as in the method of Backeberg and co-workers[19] instead of $[NH_4][O_2CEt]$–HO_2CEt due the ready commercial availability (BDH) of the former but a longer reflux time was required for the third, ring-forming, stage to optimise the yield. Also, the procedure used to isolate the product was simplified.

Bis(benzoylmethyl)butane-1,4-dioate. Succinic acid (10 g, 0.085 mol) was dissolved in MeOH (50 cm^3)–distilled water (10 cm^3). This solution was neutralised to pH 7.5 using $[NMe_3(CH_2Ph)][OMe]$ (40% solution in MeOH). The resultant solution was concentrated under reduced pressure to a volume of about 10 cm^3. Formamide (80 cm^3) was then added and the solution stirred for 5 min before addition of bromoacetophenone (37.2 g, 0.187 mol). The reaction mixture was then stirred for 48 h at room temperature, during which time a dense white solid precipitated. This was filtered off, washed with formamide (20 cm^3), water (200 cm^3) and then Et_2O (200 cm^3). The product was then dried *in vacuo* and used in the next synthetic step without further purification. Yield 18 g (60%), m.p. 140–144 °C (lit.,[18] 144–146 °C). ^{1}H NMR (200 MHz, $CDCl_3$): δ 2.7 (s, 4 H, CH_2), 5.15 (s, 4 H, CH_2) and 7.0–8.0 (m, 10 H, aryl H) (Found: C, 64.5; H, 5.4. Calc. for $C_{20}H_{20}O_7$: C, 64.5; H, 5.4%). Chemical ionisation (CI) mass spectrum: *m/z* 372 (Calc. for $C_{20}H_{18}O_6{\cdot}H_2O$: 372).

1,2-Bis(4-phenylimidazol-2-yl)ethane. Bis(benzoylmethyl) butane-1,4-dioate (10 g, 0.027 mol), $[NH_4][O_2CMe]$ (100 g, 1.30 mol) and glacial acetic acid (150 cm^3) were refluxed for 72 h

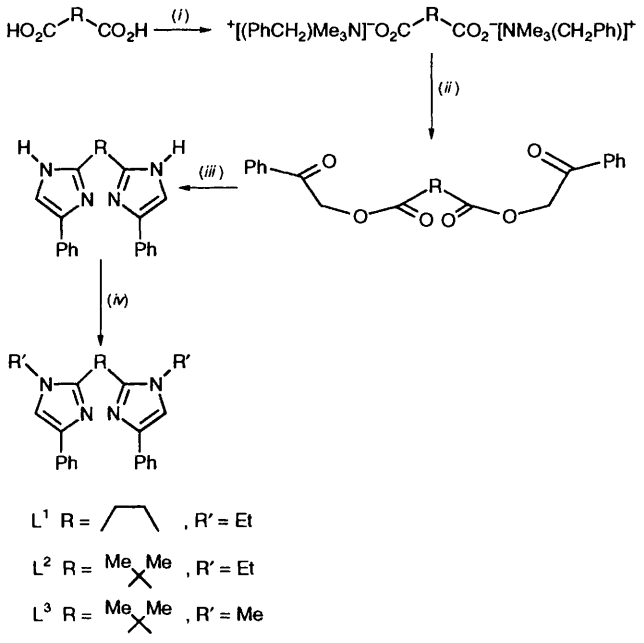

Scheme 1 Synthesis of L^1–L^3 (*i*) $[NMe_3(CH_2Ph)][OMe]$, MeOH–water; (*ii*) bromoacetophenone, $HCONH_2$; (*iii*) $[NH_4][O_2CMe]$–$MeCO_2H$, reflux; (*iv*) NaH, R′I, thf

under Ar. The resultant solution was deep red and contained a very fine orange precipitate which was filtered off through Celite. The filtrate was added dropwise to a magnetically stirred mixture of 35% NH_3 solution (150 cm^3)–water (300 cm^3) maintained at 0 °C by an ice–water bath, resulting in the precipitation of a pale brown solid which was filtered off and washed with a large volume of distilled water (500 cm^3). The crude product was recrystallised from EtOH–water (3:1) to give a microcrystalline white solid. This was filtered off, washed with EtOH (5 cm^3), Et_2O (20 cm^3) and dried *in vacuo*. Yield 2.5 g (29%), m.p. 216–219 °C (lit.,[18] 218–220 °C). ^1H NMR [$(CD_3)_2SO$ 200 MHz]; δ 3.25 (s, 4 H, CH_2), 3.5 (br s, H_2O) and 7.2–8.0 (m, 12 H aryl H) (Found: C, 68.6; H, 6.2; N, 16.2. Calc. for $C_{20}H_{18}N_4 \cdot 2H_2O$: C, 68.6; H, 6.3; N, 16.0%). CI mass spectrum: *m/z* 314 (Calc. for $C_{20}H_{18}N_4$: 314).

L^1. A suspension of 1,2-bis(4-phenylimidazol-2-yl)ethane (4.0 g, 0.0114 mol) in dry, degassed tetrahydrofuran (thf) (100 cm^3) under Ar was treated with NaH, as an 80% dispersion in mineral oil (2.4 g, 0.08 mol), in 0.25 g portions over 15 min. The reaction mixture was stirred for 20 min after the final addition to allow complete deprotonation of the bis(imidazole). Ethyl iodide (9.12 cm^3, 0.114 mol) was then added dropwise over 20 min *via* a pressure-equalising addition funnel. The solution was stirred at room temperature for 24 h to allow the reaction to proceed to completion. Quenching of the excess of NaH was effected by EtOH–Pr^iOH (2:1, 40 cm^3) which was cautiously added dropwise *via* the pressure-equalising addition funnel. The resultant solution was evaporated to dryness under reduced pressure and the residue suspended in CH_2Cl_2 (200 cm^3), causing formation of a yellow solution containing a dense white precipitate. The precipitate was filtered off and washed with two portions of CH_2Cl_2 (50 cm^3). The filtrate and washing were combined and evaporated to a volume of 50 cm^3 under reduced pressure. Toluene (15 cm^3) was added and the resultant solution allowed to evaporate over several days. Colourless prismatic crystals were formed which were filtered off, washed with toluene (5 cm^3) and dried *in vacuo*. Yield: 3.5 g (83%), m.p. 172–175 °C. ^1H NMR ($CDCl_3$, 300 MHz): δ 1.35 (t, 6 H, CH_3), 3.3 (s, 4 H, CH_2), 3.85 (q, 4 H, CH_2) and 7.0–8.0 (m, 12 H, aryl H) (Found: C, 76.0; H, 7.1; N, 14.7. Calc. for $C_{24}H_{26}N_4 \cdot 0.5H_2O$: C, 76.0; H, 7.1; N, 14.7%), Electron impact (EI) mass spectrum: *m/z* 370 (Calc. for $C_{24}H_{26}N_4$: 370).

***(b)* Bis(1-ethyl-4-phenylimidazol-2-yl)dimethylmethane (L^2).** *Bis(benzoylmethyl) 2,2-dimethylpropane-1,3-dioate.* Dimethyl malonic acid (10 g, 0.0757 mol) was dissolved in MeOH (30 cm^3)–water (10 cm^3). The resultant solution was neutralised to pH 7.5 using $[NMe_3(CH_2Ph)][OMe]$ (40% solution in MeOH), then reduced in volume to about 10 cm^3 under reduced pressure. Formamide (80 cm^3) was then added and the mixture stirred for 5 min to effect complete dissolution. Bromoacetophenone (31.65 g, 0.159 mol) was added and the mixture stirred for 24 h at room temperature, during which time the product precipitated as a dense white solid. The crude product was filtered off, washed with formamide (10 cm^3), water (200 cm^3), EtOH (20 cm^3) and Et_2O (200 cm^3) and dried *in vacuo*. It was used in the next step of the synthesis without further purification. Yield 21.4 g (55.4%), m.p. 91–94 °C (lit.,[18] 93–94 °C). ^1H NMR (200 MHz, $CDCl_3$): δ 1.7 (s, 6 H, CH_3), 5.4 (s, 4 H, CH_2) and 7.2–8.0 (m, 10 H, aryl H) (Found: C, 67.3; H, 5.3. Calc. for $C_{21}H_{20}O_6 \cdot H_2O$: C, 65.3; H, 5.5%) CI mass spectrum: *m/z* 386 (Calc. for $C_{21}H_{20}O_6 \cdot H_2O$: 386).

Dimethylbis(4-phenylimidazol-2-yl)methane. Bis(benzoylmethyl) 2,2-dimethylpropane-1,3-dioate (10 g, 0.26 mol), $[NH_4][O_2CMe]$ (125 g, 1.625 mol) and $MeCO_2H$ (180 cm^3) were refluxed for 48 h under Ar. The resultant pale yellow solution was allowed to cool to room temperature before being added dropwise to a stirred mixture of 35% NH_3 (180 cm^3)–water (360 cm^3) which was cooled by a water–ice bath, causing precipitation of the crude product as a microcrystalline white solid. This was filtered off and washed with a large volume of distilled water (500 cm^3). The crude product was then recrystallised from hot EtOH–water to give a microcrystalline white solid which was filtered off, washed with EtOH (5 cm^3), Et_2O (20 cm^3) and dried *in vacuo*. Yield 2.37 g (25.3%), m.p. 238–241 °C (lit.,[18] 240–242 °C). ^1H NMR [200 MHz, $(CD_3)_2SO$]: δ 1.9 (s, 6 H, CH_3), 3.5 (s, H_2O) and 7.2–8.0 (m, 12 H, aryl H) (Found: C, 74.4; H, 5.8; N, 16.3. Calc. for $C_{21}H_{20}N_4 \cdot H_2O$: C, 72.8; H, 6.3; N, 16.2%). CI mass spectrum: *m/z* 328 (Calc. for $C_{21}H_{20}N_4$: 328).

L^2. Dimethylbis(4-phenylimidazol-2-yl)lmethane (3.00 g, 9.09 mmol) was placed in a three-necked round bottomed flask (500 cm^3) which was purged and filled with Ar. Dry, degassed thf (100 cm^3) was added *via* a syringe. Sodium hydride, as an 80% dispersion in mineral oil (2.18 g, 0.073 mol), was carefully added to the suspension in the flask in 0.25 g portions over 15 min. The mixture was stirred for 45 min after the final addition of NaH to ensure complete deprotonation of the bis(imidazole). Ethyl iodide (7.3 cm^3, 0.09 mol) was added dropwise over 30 min *via* a pressure-equalising addition funnel. A reflux condenser was attached to the flask and the mixture refluxed for 4 h under Ar. The solution was allowed to cool to room temperature and stirred for 20 h. The excess of NaH was quenched with EtOH–Pr^iOH (2:1, 40 cm^3) which was cautiously added, dropwise, *via* the pressure-equalising addition funnel. The solution was then evaporated to dryness on a rotary evaporator and the residue suspended in CH_2Cl_2 (200 cm^3), causing formation of a pale yellow solution containing a dense white precipitate. The precipitate was filtered off and washed with two 50 cm^3 portions of CH_2Cl_2. The filtrate and washings were combined and reduced in volume to about 30 cm^3 under reduced pressure. Toluene (15 cm^3) was added and the solvent was allowed to evaporate over several days yielding colourless, block-like crystals. The product was filtered off, washed with toluene (5 cm^3) and dried *in vacuo*. Yield 2.75 g (78.8%), m.p. 193–195 °C. ^1H NMR (300 MHz, $CDCl_3$): δ 1.15 (t, 6 H, CH_3), 2.05 (s, 6 H, CH_3), 3.7 (q, 4 H, CH_2) and 7.0–8.0 (m, 12 H, aryl H) (Found: C, 78.1; H, 7.3; N, 14.6. Calc. for $C_{25}H_{28}N_4$: C, 78.1; H, 7.3; N, 14.6%) CI mass spectrum: *m/z* 385 (Calc. for $C_{25}H_{28}N_4$: 384).

***(c)* Dimethylbis(1-methyl-4-phenylimidazol-2′-yl)methane (L^3).** The first three reactions were the same as those involved in

the synthesis of L^2 (see Scheme 1); the fourth step involved methyl rather than ethyl substitution of the imidazole ring NH protons of dimethyl bis(4-phenylimidazol-2-yl), methane and MeI (5.43 cm^3, 0.087 mol) was used in the place of EtI. The crude product was dissolved in CH_2Cl_2 (30 cm^3) then transferred to a crystallising dish, toluene (15 cm^3) added and the solvent allowed to evaporate over several days, yielding a mass of very fine 'fibrous' needle-like crystals. This solid was filtered off, washed with toluene (5 cm^3) and dried *in vacuo*. Yield 2.56 g (79.1%), m.p. 234–236 °C. ^1H NMR (300 MHz, $CDCl_3$): δ 2.0 (t, 6 H, CH_3), 3.15 (s, 6 H, CH_3) and 7.0–8.0 (m, 12 H, aryl H) (Found: C, 77.1; H, 7.0; N, 15.7. Calc. for $C_{23}H_{24}N_4$: C, 77.5; H, 6.7; N, 15.7%). CI mass spectrum: *m/z* 357 (Calc. for $C_{23}H_{24}N_4$: 356).

(*d*) α,α′-Bis(4,5-diphenylimidazol-1-yl)-*o*-xylene (L^4, Scheme 2). 4,5-Diphenylimidazole (5 g, 0.0227 mol) was placed in a three-necked round-bottomed flask (500 cm^3) which was then purged and filled with Ar. Dry, degassed thf (80 cm^3) was added *via* a syringe and the mixture stirred forming a fine white suspension. Sodium hydride, as an 80% dispension in mineral oil (1.36 g, 0.045 mol), was added carefully in 0.25 g portions and, after the final addition, the mixture was stirred for 40 min to allow complete imidazolate salt formation. α,α′-Dibromo-*o*-xylene (3.00 g, 0.01 mol) was added in 0.5 g portions, leaving 5 min intervals between additions. The mixture was then refluxed for 3 h under Ar before being left to stir at room temperature for 17 h. The excess of NaH was destroyed using EtOH–Pr^iOH (2:1, 50 cm^3) which was added dropwise (**CAUTION!**) over about 15 min *via* a pressure-equalising addition funnel. The mixture was evaporated to dryness on a rotary evaporator and the residue suspended in CH_2Cl_2 (200 cm^3). The resultant suspension was shaken, then filtered and the solid on the sinter washed with CH_2Cl_2 (50 cm^3). The filtrate and washings were combined and their volume reduced to about 50 cm^3 under reduced pressure. Toluene (15 cm^3) was added and over a period of days the CH_2Cl_2 solvent was allowed to evaporate, resulting in the formation of a pure white, 'feathery' crystalline solid. This was washed with toluene (5 cm^3), Et_2O (10 cm^3), filtered off and dried *in vacuo*. Yield 3.64 g (59%), m.p. 198–200 °C. ^1H NMR (200 MHz, $CDCl_3$); δ 4.4 (s, 4 H, CH_2) and 6.6–7.4 (m, 26 H, aryl H) (Found: C, 84.1; H, 5.6; N, 10.3. Calc. for $C_{38}H_{30}N_4$: C, 84.1; H, 5.5; N, 10.3%). FAB mass spectrum: *m/z* 543 (Calc. for $C_{38}H_{30}N_4$: 542).

(*e*) α,α′-Bis(4,5-diphenylimidazol-1-yl)-*m*-xylene (L^5). The same procedure was used as for L^4, expect that α,α′-dibromo-*m*-xylene (3.00 g, 0.01 mol) was treated with the deprotonated 4,5-diphenylimidazolate salt. Yield 4.05 g (65.6%) m.p. 155–157 °C. ^1H NMR (200 MHz, $CDCl_3$): δ 4.7 (s, CH_2), 6.35 (s, 1 H, aryl H) and 6.6–7.4 (m, 25 H, aryl H) (Found: C, 82.9; H, 5.4; N, 10.1. Calc. for $C_{38}H_{30}N_4$: C, 84.1; H, 5.5; N, 10.3%). FAB mass spectrum: *m/z* 543 (Calc. $C_{38}H_{30}N_4$: 542).

Reactivity of bis(imidazole) compounds with Cu^{II}

$[CuL^1_2][BF_4]_2$. Compound L^1 (0.3 g, 8.108×10^{-4} mol) was dissolved in absolute EtOH (30 cm^3) and $Cu(BF_4)_2{\cdot}4.5H_2O$ (0.10 g, 3.24×10^{-4} mol) was added resulting in the instantaneous formation of an intense brown solution. The mixture was stirred at room temperature for 30 min, during which time a microcrystalline brown solid precipitated. This was filtered off, washed with absolute EtOH (5 cm^3), then Et_2O (5 cm^3) and dried *in vacuo*. Yield: 0.18 g (57%) (Found: C, 57.3; H, 5.0; B, 1.9; Cu, 6.0; N, 11.1. Calc. for $C_{48}H_{52}B_2CuF_8N_8$: C, 58.9; H, 5.3; B, 2.2; Cu, 6.5; N, 11.5%). Positive-ion FAB mass spectrum: *m/z* 802, $[CuL^1_2]^+$; 433, $[CuL^1]^+$; and 371, $[L^1]^+$.

$[H_2L^3][BF_4]_2$. Compound L^3 (0.20 g, 5.62×10^{-4} mol) was dissolved in CH_2Cl_2 (30 cm^3)–MeOH (5 cm^3) forming a colourless solution. The salt $Cu(BF_4)_2{\cdot}4.5H_2O$ (0.35 g, 0.001 12 mol) was added producing a pale blue solution. The mixture was stirred at room temperature for 20 min before the solvent was removed under reduced pressure yielding a pale blue solid. This was suspended in CH_2Cl_2 (15 cm^3) and stirred for 10 min at room temperature, before being filtered off, washed with absolute EtOH (10 cm^3), CH_2Cl_2 (10 cm^3), and Et_2O (10 cm^3), and dried *in vacuo*. The final product was a microcrystalline white solid. Yield: 0.19g (65%) (Found: C, 49.9; H, 4.85; B, 3.7; N, 9.9. Calc. for $C_{23}H_{26}B_2F_8N_4$: C, 51.9; H, 4.9; B, 4.1; N, 10.5%).

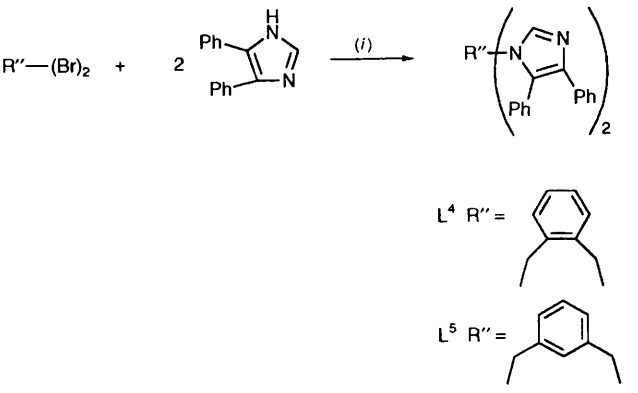

Scheme 2 Synthesis of L^4 and L^5. (*i*) NaH–thf, reflux

Compound L^2 reacted with $Cu(BF_4)_2{\cdot}4.5H_2O$ in a similar manner to that of L^3, but analytically pure material proved difficult to obtain.

$\{[CuL^4_2][BF_4]_2{\cdot}H_2O\}_n$. Compound L^4. (0.30 g, 5.54×10^{-4} mol) was dissolved in CH_2Cl_2 (20 cm^3)–MeOH (20 cm^3) $Cu(BF_4)_2{\cdot}4.5H_2O$ (0.080 g, 2.51×10^{-4} mol) was added to produce a pale blue solution. The reaction mixture was then stirred at room temperature for 20 min, and during this time a blue-grey microcrystalline solid precipitated. This was filtered off, washed with CH_2Cl_2 (5 cm^3), absolute EtOH (10 cm^3), Et_2O (5 cm^3) and dried *in vacuo*. The final product was a blue-grey powder insoluble in all common solvents (*e.g.* CH_2Cl_2, MeCN, EtOH). Yield: 0.18 g (54%) (Found: C, 67.7; H, 4.4; B, 1.5; Cu, 4.8; N. 8.3. Calc. for $C_{76}H_{60}B_2CuF_8N_8{\cdot}H_2O$: C, 68.1; H, 4.6; B, 1.6; Cu, 4.7; N, 8.4%). Positive-ion FAB mass spectrum: *m/z* 1301, $[Cu_2L^4_2(BF_4)]^+$; 1211, $[Cu_2L^4_2]^+$; 1149, $[CuL^4_2]^+$; 607, $[CuL^4]^+$; and 544, $[L^4]^+$.

$\{[CuL^5_2][BF_4]_2{\cdot}H_2O\}_n$. Compound L^5 (0.30 g, 5.54×10^{-4} mol) was dissolved in CH_2Cl_2 (20 cm^3)–absolute EtOH (20 cm^3) and $Cu(BF_4)_2{\cdot}4.5H_2O$ (0.084 g, 2.64×10^{-4} mol) was added producing a green-blue solution. The reaction mixture was then stirred at room temperature for 20 min, during which time a microcrystalline solid precipitated. This was filtered off, washed with CH_2Cl_2 (5 cm^3), Et_2O (5 cm^3) and dried *in vacuo*. The product was a pale blue-grey microcrystalline solid, insoluble in common solvents (*e.g.* CH_2Cl_2, MeCN, EtOH). Yield: 0.14 g (40%) (Found: C, 68.1; H, 4.85; B, 1.6; Cu, 5.1; N, 8.3. Calc. for $C_{76}H_{60}B_2CuF_8N_8{\cdot}H_2O$: C, 68.1; H, 4.6; B, 1.6; Cu, 4.7; N, 8.4%). Positive-ion mass spectrum: *m/z* 1297, $[Cu_2L^5_2(BF_4)]^+$; 1212, $[Cu_2L^5_2]^+$; 1148, $[CuL^5_2]^+$; 605, $[CuL^5]^+$ and 543, $[L^5]^+$.

Crystallography

A summary of the key crystallographic information is provided in Table 1. All intensity data were corrected for Lorentz, polarisation and absorption effects using the program DIFABS.[20] During data collection for each crystal the intensities of three representative reflections were measured every 150 and only in the case of $[H_2L^3][BF_4]_2$ was any decay in intensity observed and, for this compound, a linear

correction factor was applied to the data. The structures of L^1, L^2, and $[H_2L^3][BF_4]_2$ were solved by direct methods, and $[CuL^1{}_2][BF_4]_2$ by Patterson methods using the programs MITHRIL,[21] DIRDIF,[22] and SHELXS 86.[23] In each case the function minimised during full-matrix, least-squares refinement was $\Sigma w(|F_o| - |F_c|)^2$, $w = 4F_o^2/\sigma^2(F_o^2)$ using standard neutral-atom scattering factors and anomalous dispersion corrections.[24]

L^1. Colourless prismatic crystals of compound L^1 were grown by slow evaporation of solvent from a CH_2Cl_2–toluene solution and were stable in the absence of mother-liquor. The asymmetric unit consists of half the molecule of L^1, the other half being generated by rotation about a C_2 axis. The non-H atoms were refined anisotropically. The H atoms, other than those bonded to the ethyl C atoms, were found by Fourier-difference synthesis and refined isotropically. The C atoms of the ethyl groups showed high thermal motion and it was necessary to calculate the positions of associated H atoms. It was then possible to refine some of the ethyl H atoms isotropically, while others were fixed in their calculated positions and assigned isotropic thermal parameters, 20% larger than the equivalent *B* value of the C atom to which they were bound. The maximum and minimum peaks on the final Fourier-difference map corresponded to 0.24 and −0.38 e Å^{-3}, respectively.

L^2. Colourless block crystals of compound L^2 were grown by slow evaporation of solvent from a CH_2Cl_2–toluene solution, and were stable in the absence of the mother-liquor. The non-H atoms were refined anistropically. Hydrogen atoms were included in the structure-factor calculation in idealised positions (C–H 0.95 Å) and were assigned isotropic thermal parameters that were 20% larger than the equivalent *B* value of the atom to which they were bonded. The maximum and minimum peaks on the final Fourier-difference map corresponded to 0.20 and −0.19 e Å^{-3} respectively.

$[H_2L^3][BF_4]_2$. Crystals of compound L^3 grown by solvent layering and evaporation techniques using a variety of solvent combinations were all fibrous needles of a quality unsuitable for crystallographic investigation. Crystals of crystallographic quality were grown by using the tetrafluoroborate salt, which was obtained by treating L^3 with 1 equivalent of $Cu(BF_4)_2{\cdot}4.5H_2O$ (see Experimental section, above). Crystals of the salt were then grown by a layering technique in a sealed Pasteur pipette, with a MeCN solution of $[H_2L^3][BF_4]_2$ and toluene as a counter solvent. These were sensitive to loss of lattice solvent upon prolonged exposure to air, thus that used in the structure determination was mounted on a glass fibre and coated with epoxy resin, which protected the crystal and prevented any marked signs of decay during the data-collection process. All non-H atoms were refined anisotropically. The H atoms bound to N(2A), N(2B), C(4A) and C(4B) were located by Fourier-difference synthesis. The remaining H atoms were placed in idealised positions (C–H 0.95 Å), and assigned isotropic thermal parameters, 20% larger than the equivalent *B* value of the atom to which they were bonded. The maximum and minimum peaks on the final Fourier-difference map corresponded to 0.49 and −0.26 e Å^{-3}, respectively.

$[CuL^1{}_2][BF_4]_2$. Brown block crystals of $[CuL^1{}_2][BF_4]_2$ were grown by solvent evaporation from a saturated solution of the complex in absolute EtOH. The crystal used for the structure determination was mounted in a glass capillary sealed at both ends with molten wax and containing a small amount of the mother-liquor. Since it diffracted rather weakly, the atoms of the phenyl groups of the $[CuL^1{}_2]^{2+}$ cation were treated as rigid groups and refined isotropically to reduce the number of variables used in the refinement. All other non-H atoms of this fragment were refined anisotropically, and the H atoms were included in the structure-factor calculation in idealised positions (C–H 0.95 Å), and assigned isotropic thermal parameters 20% larger than the equivalent *B* value of the atom to which they were bound. The asymmetric unit also contained two $[BF_4]^-$ ions, both of which were treated as rigid groups and refined isotropically. High displacement parameters were observed for both groups, and the highest peaks in the final difference maps were associated with these groups. The maximum and minimum peaks on the final Fourier-difference map corresponded to 0.71 and −0.37 e Å^{-3}, respectively.

Atomic coordinates, thermal parameters and bond lengths and angles have been deposited at the Cambridge Crystallographic Data Centre (CCDC). See Instructions for Authors, *J. Chem. Soc., Dalton Trans.*, 1996, Issue 1. Any request to the CCDC for this material should quote the full literature citation and the reference number 186/18.

Spectroscopy

Proton NMR spectra were recorded on a Varian Gemini 200 and a Bruker AC 300 spectrometer, mass spectra using EI and CI ionisation on an IC Kratos MC25 instrument; FAB spectra using a Kratos Concept 1S spectrometer and electronic spectra on a Shimadzu UV-260 spectrophotometer. Solid-state electronic spectra were obtained by reflectance with a finely ground sample of the compound using barium sulfate as both the reference and the base material onto which the sample was loaded. The EPR spectra were recorded on a Varian E112 spectrometer at Q- (≈35) and/or X-band (≈9.25 GHz) operating frequencies with the compound under investigation contained within a quartz sample tube. For frozen-solution spectra the temperature of the sample was controlled using an Oxford Instruments ESR9 continuous-flow cryostat with a Harwell DT temperature controller and VC flowmeter. Cyclic voltammograms were recorded using an EG&G PAR 173 potentiostat and Universal Programmer. A glassy carbon working electrode, platinum-wire secondary electrode, saturated calomel reference electrode (SCE), $[NBu^n_4][BF_4]$ electrolyte, and internal ferrocene standard ($E_p = +0.56$ V, observed electrode potential *versus* SCE) were used.

Results and Discussion

Proligand crystal structures

Compound L^1 (Fig. 1) consists of discrete units of the bis(imidazole), each with C_2 point symmetry. The *N*-ethyl substitution has occurred exclusively at the N(2) position of each imidazole ring, thus locating the phenyl group substituents at the C(2) position and resulting in significant steric hindrance adjacent to the potentially co-ordinating N(1) atom. This contrasts with 1,2-bis(5-phenylimidazol-2-yl)ethane,[18] where each imidazole has the potential to co-ordinate *via* either the N(1) or N(2) atom of the heterocyclic ring, and thus the steric hindrance from the phenyl groups may be on the carbon atom immediately adjacent to the co-ordinating nitrogen atom or one carbon removed. Fig. 1 shows that, in the solid state, the bis(imidazole) molecule adopts a conformation where the pair of phenyl and ethyl substituents in each molecule orientate themselves in a quasi-antiparallel manner, presumably to minimise intramolecular steric interactions.

The crystal structure of compound L^2 (Fig. 2) contains discrete units of the molecule and shows that *N*-ethyl substitution has occurred solely at the N(1A) and N(1B) imidazole ring positions, thus positioning the phenyl rings adjacent to the potential donor nitrogens atoms [N(2A), N(2B)]. The conformation adopted by the molecules in the crystals involves two sets of phenyl and ethyl substituents on the two imidazole rings of each L^2 molecule orientated in a quasi-antiparallel manner to minimise steric interactions between these groups. Furthermore, the two imidazole rings are also

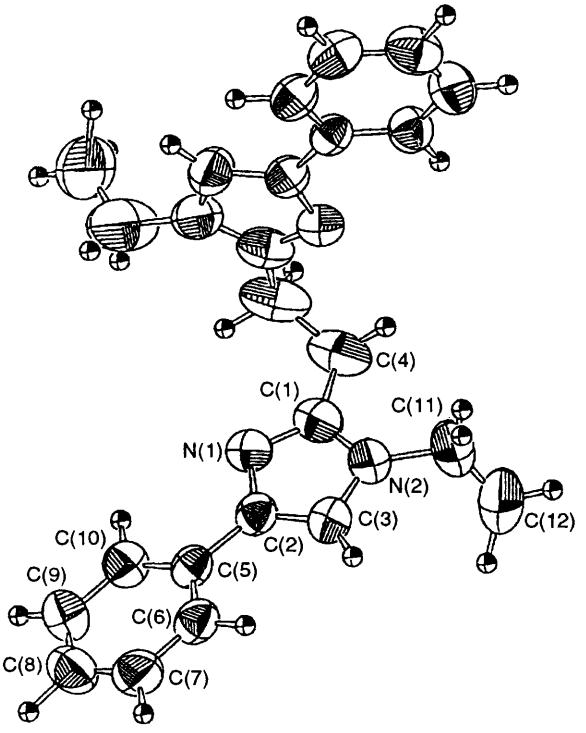

Fig. 1 An ORTEP[25] view of the L^1 molecule showing the atom numbering scheme

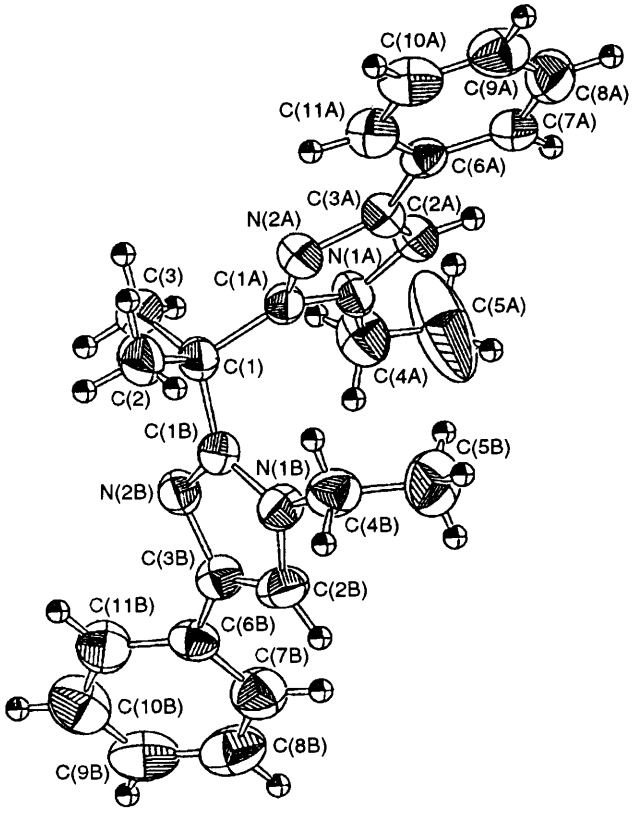

Fig. 2 An ORTEP view of the compound L^2 showing the atom numbering scheme

staggered with respect to the dimethyl substitution on the bridging carbon, again presumably to minimise steric interactions between the substituents on the imidazole rings and the dimethyl substitution on the carbon bridging group.

Crystal structure of $[H_2L^3][BF_4]_2$·MeCN

The crystal structure of $[H_2L^3][BF_4]_2$·MeCN (Fig. 3) contains discrete units of $[H_2L^3]^{2+}$ with one molecule of

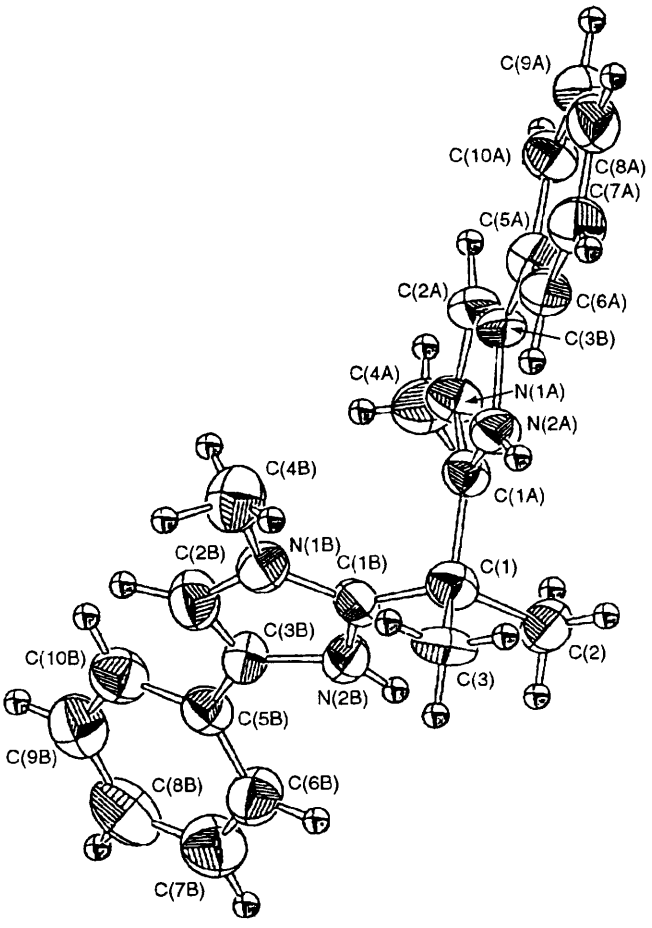

Fig. 3 An ORTEP view of the $[H_2L^3]^{2+}$ cation showing the atom numbering scheme

MeCN lattice solvent and two $[BF_4]^-$ anions per $[H_2L^3]^{2+}$. The lattice MeCN is well removed from the $[H_2L^3]^{2+}$ and $[BF_4]^-$ ions. The $[BF_4]^-$ anions are linked by hydrogen bonds to the protonated nitrogen atoms of the $[H_2L^3]^{2+}$ [H(1A)···F(1) 2.056, H(1B)···F(3) 2.287, H(1B)···F(6) 2.379 Å]. The *N*-methyl substitution of L^3 has occurred purely at the N(1A) and N(1B) ring positions. This is attributed to the considerable steric hindrance in the vicinity of the N(2A) and N(2B) ring positions which effectively inhibits any possibility of reaction at these atoms (*cf.* the L^2 and L^1 syntheses). The conformation adopted by the $[H_2L^3]^{2+}$ again appears to minimise intramolecular steric interactions. The two imidazole rings of each molecule are twisted with respect to each other, reducing the steric interactions between them and their substituents, and between these substituents and the dimethyl substitution on the carbon bridge of the molecule, as observed in L^2 (see above).

Crystal structure of $[CuL^1_2][BF_4]_2$

The crystal structure of $[CuL^1_2][BF_4]_2$ consists of $[CuL^1_2]^{2+}$ cations (Fig. 4) and $[BF_4]^-$ anions. The co-ordination sphere about each Cu^{II} comprises four N-co-ordinated imidazole rings from two L^1 ligands. The Cu^{II}–N bond lengths (Table 2, average 2.01 Å) are in good agreement with values observed in other copper(II) tetrakis(imidazole) complexes.[8,12,16,18,27] The $[BF_4]^-$ anions are > 3.5 Å from the metal atom. The co-ordination geometry of the metal in $[CuL^1_2]^{2+}$ is virtually square planar with N–Cu–N bond angle deviations less than 2.5° from 90° (see Table 2) and the Cu^{II} is displaced only 0.022 Å out of the N_4 plane. The dihedral angles between the imidazole and CuN_4 least-squares plane are 60.11 (A), 54.06 (B), 59.45 (C), and 53.62° (D). Thus, all of the imidazole rings are similarly orientated with respect

to the CuN_4 plane, with the *trans* rings being essentially parallel. The observed dihedral angles are smaller than those seen in $[Cu(1,4,5\text{-tmim})_4][ClO_4]_2$[12] (75.5 and 75.7°) and $[Cu(Him)_4(NO_3)_2]$[12] (81.4 and 85.4°), but are larger than those of $[Cu(bpip)_2][ClO_4]_2 \cdot 4MeOH$[18] (34.0 and 34.3°) where bpip is 2,2-bis(5-phenylimidazol-2-yl)propane. In contrast, for $[Cu(Him)_4(SO_4)]$[12] and $[Cu(Him)_4][ClO_4]_2$[12] the two pairs of dihedral angles between the imidazole and CuN_4 planes are dissimilar (81.0 and 29.7 and 85.7 and 18.7°, respectively). The orientation of the imidazole with respect to the metal–ligand axes influences the interaction of the imidazole π orbitals and the copper(II) 3d orbitals and this can affect the electronic structure of the $[Cu(imidazole)_4]^{2+}$ centre (see below).

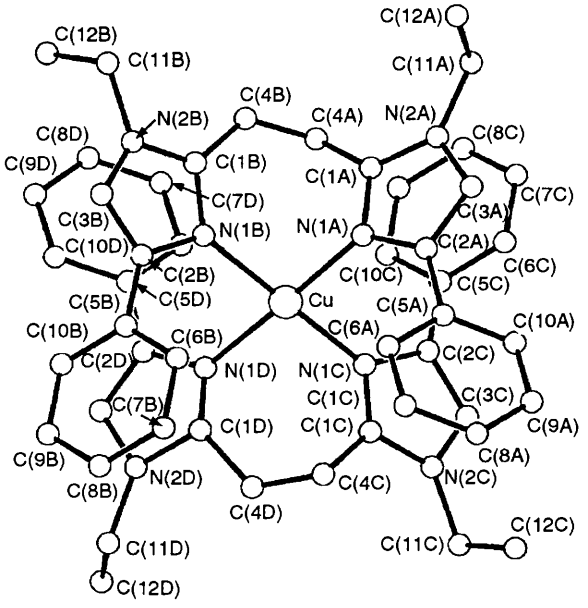

Fig. 4 A PLUTO[26] view of the $[CuL^1_2]^{2+}$ cation showing the atom numbering scheme and stacking of the *trans*-adjacent imidazole and phenyl rings

Table 3 indicates that the individual phenylimidazole units are not coplanar, in contrast to the related system $[Cu(bpip)_2][ClO_4]_2 \cdot 4MeOH$[18] which involves dihedral angles of 1.3 and 4.2° between the imidazole ring plane and the 5-phenyl ring substituents. The dihedral angles between the phenyl ring planes on opposite sides of the $[CuL^1_2]^{2+}$ unit are small (between phenyl planes B and C 4.52° and between A and D 4.31°). This, together with the arrangement of the imidazole rings, indicates the $[CuL^1_2]^{2+}$ unit almost has *i* point symmetry. Table 4 also shows that, between phenyl plane B and imidazole plane D, and between phenyl plane C and imidazole plane A, the dihedral angles are small (< 10°), *i.e.* these planes are almost parallel. The distance between C(5B) and N(1D) is 3.28 Å, and between the C(5C) and N(1A) is 3.29 Å, implying the presence of intramolecular π-stacking interaction between these two pairs of planes.[28] This observation is clearly illustrated in Fig. 4. [This stacking will be referred to as *trans*-adjacent stacking since each co-ordinated imidazole is covered by a phenyl ring from the other bis(imidazole) ligand of the CuN_4 complex.]. The intramolecular *trans*-adjacent imidazole/phenyl ring π-stacking effect is presumably (partly) responsible for the lack of coplanarity in individual phenylimidazole units in $[CuL^1_2]^{2+}$. In contrast, in $[Cu(bpip)_2][ClO_4]_2 \cdot 4MeOH$,[18] the phenyl substituents of the bpip ligand are each located at the 5 imidazole ring position and are thus not adjacent to the co-ordinating N atom so that the phenyl substituents are pointing quasi-radially out from the complex preventing an intramolecular parallel stacking interaction. Furthermore, the steric interactions between the imidazole A, B, C, D and phenyl substituent C, D, A, B rings, respectively, may be responsible for the slight rhombic distortion of the co-ordination geometry of $[CuL^1_2]^{2+}$. The copper(II) centre of $[Cu(bpip)_2][ClO_4]_2 \cdot 4MeOH$[18] is tetragonal and the steric interactions between the radially orientated 5-phenyl rings and the adjacent co-ordinated imidazole ring in this complex are negligible. In $[CuL^1_2][BF_4]_2$, for an exact square-planar geometry, the

Table 1 Crystallographic data*

	L^1	L^2	$[H_2L^3][BF_4]_2 \cdot MeCN$	$[CuL^1_2][BF_4]_2$
Formula	$C_{24}H_{26}N_4$	$C_{25}H_{28}N_4$	$C_{25}H_{29}B_2F_8N_5$	$C_{48}H_{52}B_2CuF_8N_8$
M	370.5	384.52	573.14	978.15
Space group	*C*2/*c*	*Pna*2$_1$	*P*2$_1$/*c*	*Pca*2$_1$
Crystal system	Monoclinic	Orthorhombic	Monoclinic	Orthorhombic
a/Å	19.500(2)	19.10(1)	10.919(3)	25.22(3)
b/Å	9.701(1)	8.69(1)	24.981(2)	8.65(3)
c/Å	10.618(1)	13.04(6)	10.241(2)	21.65(4)
β/°	96.47(1)		95.35(2)	
U/Å^3	1996.0(4)	2165(10)	2781(2)	4726(28)
D_c/g cm^{-3}	1.233	1.179	1.369	1.375
F(000)	792	824	1184	2028
Crystal size/mm	0.65 × 0.50 × 0.25	0.60 × 0.60 × 0.60	0.25 × 0.25 × 0.45	0.40 × 0.40 × 0.25
λ/Å	1.541 78 (Cu-Kα)	0.710 69 (Mo-Kα)	1.541 78 (Cu-Kα)	0.710 69 (Mo-Kα)
μ/cm^{-1}	5.41	0.66	10.15	5.34
Diffractometer	Rigaku AFC5R	Rigaku AFC6S	Rigaku AFC5R	Rigaku AFC6S
Data collection	ω–2θ	ω–2θ	ω–2θ	ω
T/°C	22 ± 1	23 ± 1	22 ± 1	23 ± 1
Scan rate/° min^{-1}	32.0	8.0	16.0	2.0
in ω	2 Rescans	3 Rescans	2 Rescans	3 Rescans
Scan width/°	1.47 + 0.30 tan θ	1.52 + 0.30 tan θ	1.21 + 0.30 tan θ	0.88 + 0.30 tan θ
$2\theta_{max}$/°	120.1	50.1	120.1	50.0
No. reflections				
Total	1638	2214	4582	4676
Unique	1584	2214	4266	4665
Structure solution	Direct methods	Direct methods	Direct methods	Patterson
No. data used in refinement	1295	1287	2615	1693
Data : parameter ratio	7.57	4.91	7.24	5.18
Final *R*	0.072	0.049	0.083	0.084
Final *R'*	0.102	0.069	0.102	0.096

* Details in common: $Z = 4$; graphite monochromator; weighting scheme $4F_o^2/\sigma^2(F_o^2)$.

Table 2 Selected bond lengths (Å) and angles (°) for $[CuL^1{}_2][BF_4]_2$ with estimated standard deviations (e.s.d.s) in parentheses

Co-ordination sphere							
Cu–N(1A)	2.00(2)	Cu–N(1B)	2.05(2)	N(1A)–Cu–N(1B)	90.2(8)	N(1B)–Cu–N(1D)	89.3(8)
Cu–N(1C)	1.94(2)	Cu–N(1D)	2.06(2)	N(1A)–Cu–N(1C)	88.3(8)	N(1C)–Cu–N(1D)	92.3(9)
				N(1A)–Cu–N(1D)	176.9(9)	N(1B)–Cu–N(1C)	178.4(8)
Imidazole Rings							
N(1A)–C(1A)	1.38(3)	N(2C)–C(1C)	1.40(4)	C(1A)–N(1A)–C(2A)	108(2)	C(1C)–N(2C)–C(3C)	105(3)
N(1B)–C(1B)	1.36(3)	N(2D)–C(1D)	1.42(4)	C(1B)–N(1B)–C(2B)	106(2)	C(1D)–N(2D)–C(3D)	100(3)
N(1C)–C(1C)	1.31(4)	N(2A)–C(3A)	1.31(4)	C(1C)–N(1C)–C(2C)	108(2)	N(2A)–C(3A)–C(2A)	111(2)
N(1D)–C(1D)	1.21(5)	N(2B)–C(3B)	1.27(3)	C(1D)–N(1D)–C(2D)	109(3)	N(2B)–C(3B)–C(2B)	110(2)
N(1A)–C(2A)	1.36(3)	N(2C)–C(3C)	1.33(4)	N(1A)–C(1A)–N(2A)	108(2)	N(2C)–C(3C)–C(2C)	112(3)
N(1B)–C(2B)	1.39(3)	N(2D)–C(3D)	1.39(3)	N(1B)–C(1B)–N(2B)	107(2)	N(2D)–C(3D)–C(2D)	109(2)
N(1C)–C(2C)	1.43(3)	C(2A)–C(3A)	1.41(4)	N(1C)–C(1C)–N(2C)	111(2)	C(3A)–C(2A)–N(1A)	106(2)
N(1D)–C(2D)	1.34(4)	C(2B)–C(3B)	1.34(4)	N(1D)–C(1D)–C(2D)	113(3)	C(3B)–C(2B)–N(1B)	106(2)
N(2A)–C(1A)	1.40(4)	C(2C)–C(3C)	1.40(4)	C(1A)–N(2A)–C(3A)	107(2)	C(3C)–C(2C)–N(1C)	104(2)
N(2B)–C(1B)	1.33(3)	C(2D)–C(3D)	1.33(4)	C(1B)–N(2B)–C(3B)	111(2)	C(3D)–C(2D)–N(1D)	108(2)
Ligand Bridge							
C(1A)–C(4A)	1.43(5)	C(1C)–C(4C)	1.44(4)	N(1A)–C(1A)–C(4A)	123(2)	N(2C)–C(1C)–C(4C)	116(3)
C(4A)–C(4B)	1.40(5)	C(4C)–C(4D)	1.35(5)	N(1B)–C(1B)–C(4B)	126(2)	N(2D)–C(1D)–C(4D)	109(3)
C(4B)–C(1B)	1.43(4)	C(4D)–C(1D)	1.60(6)	N(1C)–C(1C)–C(4C)	132(3)	C(1A)–C(4A)–C(4B)	122(3)
				N(1D)–C(1D)–C(4D)	137(3)	C(1B)–C(4B)–C(4A)	126(3)
				N(2A)–C(1A)–C(4A)	129(3)	C(1C)–C(4C)–C(4D)	118(3)
				N(2B)–C(1B)–C(4B)	127(2)	C(1D)–C(4D)–C(4C)	125(3)

Tables 3 Dihedral angles (°) between least-squares phenyl ring planes and imidazole planes of $[CuL^1{}_2][BF_4]_2$*

	Imidazole plane			
Phenyl plane	A	B	C	D
A	40.46	28.96	24.63	45.84
B	3.77	59.92	59.55	8.12
C	5.28	59.28	58.39	12.26
D	38.49	26.37	22.64	43.30

* The imidazole planes are defined in Fig. 4, and the phenyl planes are labelled on the basis of which imidazole group to which they are bound.

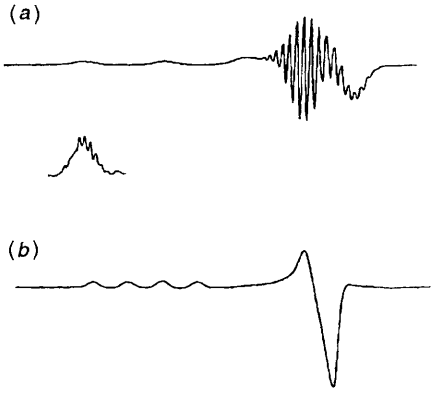

Fig. 5 The X-(*a*) and Q-band (*b*) EPR spectra of $[CuL^1{}_2][BF_4]_2$ in CH_2Cl_2–toluene at 77 K. Insert shows magnification of first copper-hyperfine split g_z absorption

imidazole A, B, C, D and phenyl C, D, A, B rings would have to clash, and distortion of the copper(II) co-ordination geometry (from D_{4h} to D_2) relieves this steric interaction (Fig. 4).

Electron paramagnetic resonance studies

$[CuL^1{}_2][BF_4]_2$. The X-band powder EPR spectrum of $[CuL^1{}_2][BF_4]_2$ has slight rhombic, almost tetragonal character, consistent with the crystal structure of the complex. The $g_{\|}$ resonance (2.214) would be expected to be split into four lines due to copper-hyperfine interactions; the first two of these are clearly resolved ($A_{\|}$ = 190 G, 196 × 10^{-4} cm^{-1}), the third is superimposed on, and the fourth is completely obscured by, the $g_{\perp}$ region of the spectrum ($g_{\perp}$ = 1.967). The X-band EPR spectrum in CH_2Cl_2–toluene at 77 K [Fig. 5(*a*)] is very similar to that for the solid state; $g_{\|}$ = 2.223, $A_{\|}$ = 190 G, 197 × 10^{-4} cm^{-1}. The copper-hyperfine splittings in this region of the spectrum are further split due to nitrogen-superhyperfine coupling, six of which are resolved in the first $g_{\|}$ line of the spectrum [see Fig. 5(*a*)]. The $g_{\perp}$ region of the spectrum clearly displays an overshoot line[29] with an estimated g value of 1.97, as well as the 'real' $g_{\perp}$ absorption with an approximate g value of 2.05. Again this region of the spectrum shows considerable superhyperfine splitting due to interaction with the imidazole ligand nitrogen atoms, and the splittings are particularly well resolved. The Q-band EPR spectrum in CH_2Cl_2–toluene at 77 K [Fig. 5(*b*)] resolves g_x = 2.034 and g_y = 2.052. The g_z absorption (2.229) is split by copper-hyperfine interactions into four equally spaced lines (all of which are resolved) with a hyperfine coupling constant, A_z, of 190 G (198 × 10^{-4} cm^{-1}).

$\{[CuL^4{}_2][BF_4]_2{\cdot}H_2O\}_n$. The insolubility of this compound confined Q-band EPR investigations to finely powdered samples. The parameters $g_{\|} \approx 2.210$, $A_{\|} \approx 180$ G (186 × 10^{-4} cm^{-1}), and $g_{\perp} \approx 2.030$ are very similar to those of $[CuL^1{}_2][BF_4]_2$, consistent with these materials have very similar geometries at their copper(II) centres.

$\{[CuL^5{}_2][BF_4]_2{\cdot}H_2O\}_n$. Owing to the insolubility of $\{[CuL^5{}_2][BF_4]_2{\cdot}H_2O\}_n$, Q-band EPR spectra were only taken on finely ground samples of the compound. The spectrum is characteristic of a tetragonal copper(II) centre. The $g_{\|}$ and $g_{\perp}$ regions are clearly resolved with the $g_{\|}$ absorption being split into four lines due to copper-hyperfine couplings, all four lines of which are observed: $g_{\|} \approx 2.214$, $A_{\|} \approx 180$ G (186 × 10^{-4} cm^{-1}), and $g_{\perp} \approx 2.030$. These values are similar to those of $[CuL^1{}_2][BF_4]_2$.

Electronic spectroscopy

Table 4 shows the peak positions of the electronic spectra of $[CuL^1{}_2][BF_4]_2$ in both CH_2Cl_2 solution and the solid state and the proposed assignments. The three lowest-energy bands display very similar energies in both media, consistent with the inference made from the EPR data (see above) that this compound maintains its solid-state structure in solution. The spectrum in CH_2Cl_2 exhibits two absorptions at 19 600

Table 4 Electronic spectral data for bis(imidazole) compounds and their copper(II) complexes together with proposed assignments

	CH_2Cl_2 solution		Solid state	
System	$\tilde{\nu}$/cm^{-1}	ε/dm^3 mol^{-1}	$\tilde{\nu}$/cm^{-1}	Proposed assignment
L^1	37 050	32 700	—	Phenyl, $\pi \longrightarrow \pi^*$
$[CuL^1{}_2][BF_4]_2$	*ca.* 43 000[a]	32 300		Ethylimidazole, $\pi \longrightarrow \pi^*$
				n(imidazole) $\longrightarrow$ Cu^{II}
			39 400	Phenyl, $\pi \longrightarrow \pi^*$
			32 900 (sh)	Imidazole (π_2) $\longrightarrow$ Cu^{II}
	27 600	1230	27 200	Imidazole (π_1) $\longrightarrow$ Cu^{II}
	19 600 (sh)	92	19 000 (sh)	d–d
	15 600 (sh)	23	15 800 (sh)	d–d
L^5	38 300	24 100	—	Phenyl, $\pi \longrightarrow \pi^*$
$\{[CuL^5{}_2][BF_4]_2{\cdot}H_2O\}_n$[b]	—	—	39 400	Phenyl, $\pi \longrightarrow \pi^{*+}$
				Imidazole (π_1) $\longrightarrow$ Cu^{II}
				Imidazole (π_2) $\longrightarrow$ Cu^{II}
	—	—	18 450 (sh)	d–d
L^4	38 500	30 000	—	Phenyl, $\pi \longrightarrow \pi^*$
$\{[CuL^4{}_2][BF_4]_2{\cdot}H_2O\}_n$[b]			39 400	Phenyl, $\pi \longrightarrow \pi^{*+}$
				Imidazole (π_2) $\longrightarrow$ Cu^{II}
			29 200 (sh)	Imidazole (π_1) $\longrightarrow$ Cu^{II}
	—	—	16 400	d–d

[a] Only observed up to the solvent cut-off of *ca.* 43 500 cm^{-1}. [b] The insolubility of the $\{[CuL^4{}_2][BF_4]_2{\cdot}H_2O\}_n$ and $\{[CuL^5{}_2][BF_4]_2{\cdot}H_2O\}_n$ prevented recording of solution spectra.

(ε = 92) and 15 600 cm^{-1} (23 dm^3 mol^{-1} cm^{-1}) which are attributed to d–d transitions. The first is of a higher energy than the d–d bands of the solution spectra of other $[Cu(imidazole)_4]^{2+}$ complexes, *e.g.* $[Cu(1,4,5\text{-tmim})_4][ClO_4]_2$ [16 800 cm^{-1} (ε = 50 dm^3 mol^{-1} cm^{-1}) in MeOH][12] and $[Cu(1,2\text{-dmim})_4][ClO_4]_2$ [16 800 cm^{-1} (ε = 50 dm^3 mol^{-1} cm^{-1}) in MeOH], where 1,2-dmim is 1,2-dimethylimidazole,[12] but rather similar to the d–d bands in mull (solid-state) spectra of these compounds at 80 K, $[Cu(1,4,5\text{-tmim})_4][ClO_4]_2$ ($\approx$20 000 and $\approx$16 900 cm^{-1}),[12] $[Cu(1,2\text{-dmim})_4][ClO_4]_2$ ($\approx$19 000 cm^{-1}).[12]

A solution of $[CuL^1{}_2][BF_4]_2$ in CH_2Cl_2 also exhibits an absorption at 27 600 cm^{-1} (ε = 1230 dm^3 mol^{-1} cm^{-1}). Other $[Cu(imidazole)_4]^{2+}$ complexes manifest an absorption in this region and these have been assigned to π-imidazole to Cu^{II} ligand to metal charge transfer (l.m.c.t.), probably promotion from the highest-occupied molecular orbital (HOMO) π_1 of the imidazole (which primarily has carbon $2p_\pi$ character).[10–12] The intensity of this band in these complexes shows some dependence upon the orientation of the imidazole rings with respect to the CuN_4 plane, as demonstrated for $[CuL^1{}_2][BF_4]_2$, $[Cu(1,4,5\text{-tmim})_4][ClO_4]_2$,[12] and $[Cu(bpip)_2][ClO_4]_2$.[18] The solid-state structures of these $[Cu(imidazole)_4]^{2+}$ centres have (average) values of the dihedral angle between the imidazole and the CuN_4 plane of 56.8, 75.6, and 34.2°, respectively, and exhibit absorptions at *ca.* 27 600 cm^{-1} (ε = 1230 dm^3 mol^{-1} cm^{-1}) in CH_2Cl_2, 28 700 cm^{-1} (ε = 1880 dm^3 mol^{-1} cm^{-1}) in MeOH, and 25 600 cm^{-1} (ε = 205 dm^3 mol^{-1} cm^{-1}) in MeOH. Thus, assuming that the orientation of the imidazole rings observed in the solid state is maintained in solution, the intensity of this transition increases as the imidazole rings assume a more perpendicular orientation with respect to the CuN_4 plane. Using a simplified D_{4h} $[Cu(imidazole)_4]^{2+}$ centre, where im is a five-membered ring, containing only one (the co-ordinated) nitrogen atom, the lowest unoccupied molecular orbital (LUMO) is $d_{x^2-y^2}$ (B_{1g}) and the HOMO π orbital is spatially symmetrical about the upper and lower faces of the ring with each face encompassing only one orbital phase (either positive or negative). For imidazole rings orientated perpendicular to the CuN_4 plane the four HOMO π orbitals transform as $A_{2g} + B_{2g} + E_u$, which indicates that the π-imidazole to Cu^{II} l.m.c.t. transition should be (x,y) polarised. For imidazole rings orientated parallel to the CuN_4 plane the four HOMO π orbitals transform as $E_g + A_{2u} + B_{2u}$, and thus the π-imidazole to Cu^{II} l.m.c.t. transition is z-polarised. The σ transition [n(imidazole) to Cu^{II} l.m.c.t. in the x,y plane is strongly allowed, and intensity stealing from this transition should enhance the intensity of the x,y-polarised in-plane π-imidazole to Cu^{II} l.m.c.t. transition (see above), but not the z-polarised transition.[12] Thus, the closer the imidazole rings of a $[Cu(imidazole)_4]^{2+}$ complex are orientated perpendicular to the CuN_4 plane, the larger is the intensity of the π_1-imidazole to Cu^{II} l.m.c.t. transition, as described above.

The highest-energy feature observed in the electronic spectrum of $[CuL^1{}_2][BF_4]_2$ in CH_2Cl_2 is a very broad intense absorption which commences at *ca.* 33 300 cm^{-1} and continues to the solvent cut-off point of *ca.* 43 500 cm^{-1}, and probably contains several transitions including phenyl, $\pi \longrightarrow \pi^*$. Thus, the electronic spectrum of L^1 in CH_2Cl_2 solution possesses an intense band at *ca.* 37 000 cm^{-1} (ε = 30 000 dm^3 mol^{-1} cm^{-1}), *cf.* bpip in MeOH solution, λ_{max} = 37 500 cm^{-1} (ε = 33 800 dm^3 mol^{-1} cm^{-1}), assigned to phenyl, $\pi \longrightarrow \pi^*$ transitions.[18]

Three imidazole to Cu^{II} d orbital c.t. transitions are expected in the electronic spectrum of a $[Cu(imidazole)_4]^{2+}$ complex: n(imidazole) $\longrightarrow$ Cu^{II}, π_2(imidazole) $\longrightarrow$ Cu^{II}, and π_1(imidazole) $\longrightarrow$ Cu^{II} (in increasing order of transition energy) although, in practice, both the first two can overlap with (and thus be obscured by) ligand $\pi \longrightarrow \pi^*$ transitions[12,18] (in the case of L^1, for both the imidazole and phenyl rings). These transitions would be expected to be red-shifted in N/C-alkyl/phenyl imidazole ring-substituted copper(II) complexes, relative to unsubstituted imidazole tetrakis-copper(II) complexes, due to destabilisation of the n, π_2 and π_1 imidazole MOs by the electron-donating effects of the ring substitution.[12] The destabilisation of the n, π_1, π_2 MOs of alkylated imidazoles relative to unsubstituted imidazole is clearly evinced in the electronic spectra of $[CuL^1{}_2][BF_4]_2$ (in both solid and CH_2Cl_2 solution), the π_1 to Cu^{II} c.t. band of which is red-shifted compared to those of the unsubstituted imidazole complexes, $[Cu(Him)_4(NO_3)_2]$[8] and $[Cu(Him)_4(SO_4)]$.[9] For the $\pi_1 \longrightarrow Cu^{II}$ c.t. band of $[CuL^1{}_2][BF_4]_2$ [27 200 (solid), 27 600 cm^{-1} (CH_2Cl_2)], the red shift is *ca.* 7000 cm^{-1} relative to $[Cu(Him)_4(NO_3)_2]$[8] and *ca.* 5500 and 2700 cm^{-1} for the split transition of $[Cu(Him)_4(SO_4)]$.[9]

The band positions and assignments of the solid-state electronic spectra of $\{[CuL^4{}_2][BF_4]_2{\cdot}H_2O\}_n$ and $\{[CuL^5{}_2][BF_4]_2{\cdot}H_2O\}_n$ are shown in Table 4 and the assignments

were made by comparison to $[CuL^1{}_2][BF_4]_2$ and other tetrakis(imidazole) copper(II) complexes.[9–12] The d–d band of $\{[CuL^5{}_2][BF_4]_2{\cdot}H_2O\}_n$ is similar in energy to the higher-energy d–d band of $[CuL^1{}_2][BF_4]_2$ ($\approx 19\,000$ cm^{-1}, reflectance spectrum, Table 4), $[Cu(1,4,5\text{-tmim})_4][ClO_4]_2$ ($\approx 19\,000$ cm^{-1}, mull at 80 K),[12] and the d–d bands of $[Cu(Him)_4(NO_3)_2]$ ($\approx 19\,000$ cm^{-1}, mull at 80 K)[12] and $[Cu(1,2\text{-dmim})_4][ClO_4]_2$ ($\approx 19\,000$ cm^{-1}, mull at 80 K).[12] The observed d–d absorption of $\{[CuL^5{}_2][BF_4]_2{\cdot}H_2O\}_n$ is similar in energy to the lower-energy d–d band of $[CuL^1{}_2][BF_4]_2$ ($\approx 15\,800$ cm^{-1}, reflectance spectrum, Table 4 and $[Cu(1,4,5\text{-tmim})_4][ClO_4]_2$ ($\approx 16\,900$ cm^{-1}, mull at 80 K).[12] This strongly suggests that the chromophores of $\{[CuL^4{}_2][BF_4]_2{\cdot}H_2O\}_n$ and $\{[CuL^5{}_2][BF_4]_2{\cdot}H_2O\}_n$ have $[Cu(imidazole)_4]^{2+}$, square-planar, CuN_4 centres.

Electrochemistry of $[CuL^1{}_2][BF_4]_2$

The cyclic voltammogram of the L^1 ligand in CH_2Cl_2 solution at a scan rate of 0.1 V s^{-1} in the scan ranges 0 to +1.8 and −2.0 to 0 V [Fig. 6(*a*)] exhibited a distorted irreversible oxidation at +1.3 V. The cyclic voltammogram of a CH_2Cl_2 solution of $[CuL^1{}_2][BF_4]_2$ at a scan rate of 0.2 V s^{-1} in the voltage ranges from +1.2 to +1.8 and −1.6 to +1.2 V is shown in Fig. 6(*b*). On the forward scan from +1.2 to +1.8 V an irreversible oxidation peak was observed at +1.49 V, superimposed on the solvent breakdown current surge which is attributed to ligand oxidation. On scanning from +1.8 to −1.6 V a strong reduction feature was seen at −0.07 V and on the return scan from −1.8 to +1.2 V an oxidation step was observed at +0.74 V, plus a small feature at +0.900 V. An 0.2 V s^{-1} scan in the voltage range +1.2 to +0.4 to +1.2 V revealed no electrochemical activity in this range, indicating that the −0.07 V reduction and +0.74 V oxidation are coupled, and these redox processes are attributed to the $[CuL^1{}_2]^{2+/+}$ couple. This supposition was supported using the technique of controlled-potential spectroelectrolysis in which a CH_2Cl_2 solution of $[CuL^1{}_2][BF_4]_2$ was subjected to a continuous potential of −0.7 V for 45 min; this effected complete reduction of the complex, as indicated by the change from a brown solution to very pale yellow, the electronic spectrum of which confirmed the loss of the characteristic copper(II) d–d bands.

A solution of $[CuL^1{}_2][BF_4]_2$ in CH_2Cl_2 was scanned from +1.2 to −0.6 and then from −0.6 + 1.2 V, at several scan rates ranging from 0.1 to 1.2 V s^{-1}. This resulted in the difference in peak potential values (ΔE_p) increasing from 0.76 (at 0.1) to 0.96 V (at 1.2 V s^{-1}). This behaviour, coupled with the large anodic peak–cathodic peak separation, clearly indicates that the redox couple is quasi-reversible[30] in character.

Table 5 shows the reduction potentials, $E_{\frac{1}{2}}$, for several $[Cu(imidazole)_4]^{2+}$–$[Cu(imidazole)_4]^{+}$ couples. For all of these systems (nearly) reversible electrochemical behaviour[32] and/or fast self-exchange rates[31,33,35] are observed for the Cu^{II}–Cu^{I} couple. Structural characterisation of the Cu^{II} and Cu^{I} oxidation states of $[CuL^6{}_2]^{n+}$ and $[CuL^7{}_2]^{n+}$ (n = 2 or 1) indicates that the molecular structures in each oxidation state are similar,[16,31] with flattened tetrahedral co-ordination geometries intermediate between those preferred by Cu^{II} (square-planar) and Cu^{I} (tetrahedral). Thus, for these two complexes the small reorganisational energy required for a $Cu^{II} \longleftrightarrow Cu^{I}$ redox reaction favours facile electron transfer. For $[CuL^{10}]^{n+}$ (n = 2 or 1) fast electron transfer [self-exchange rate, $k \geqslant 1.76 \times 10^4$ dm^3 mol^{-1} s^{-1} (MeCN)][33] is observed, even though there are quite large structural differences between the solid state copper-(II) and -(I) molecular structures [*e.g.* average bond lengths increase by 0.12 Å, from Cu^{II} to Cu^{I}, although in an asymmetric manner; also there is a geometric rearrangement from Cu^{II} (distorted square pyramidal) to Cu^{I} (trigonal bipyramidal)].[33] For $[CuL^{11}]^{n+}$ (n = 2 or 1) fast electron transfer is observed ($k \leqslant 5 \times 10^5$ dm^3 mol^{-1} s^{-1}) despite there being a postulated co-ordination number change upon $Cu^{II} \longleftrightarrow Cu^{I}$ redox reaction.[35] Taking into account the electrochemical properties of these related systems, a possible explanation for the pronounced quasi-reversible electrochemical behaviour of $[CuL^1{}_2][BF_4]_2$ is that the *trans*-adjacent imidazole/phenyl ring π-stacking interactions (see above, Fig. 4) effectively 'lock' the copper(II) co-ordination geometry. Thus, for rearrangement to a co-ordination geometry more amenable to Cu^{I} (more tetrahedral) the interactions associated with the *trans*-adjacent imidazole and phenyl rings would be inhibiting.

The complex $[CuL^1{}_2][BF_4]_2$ displays considerably more positive oxidation and reduction redox properties $\{E'_{\frac{1}{2}}([CuL^1{}_2][BF_4]_2) = [(-0.07) + (+0.74)]/2 = +0.335$ V at 0.2 V s$^{-1}\}$ relative to all but one of the systems in Table 5. This observation can be tentatively rationalised in terms of the π-

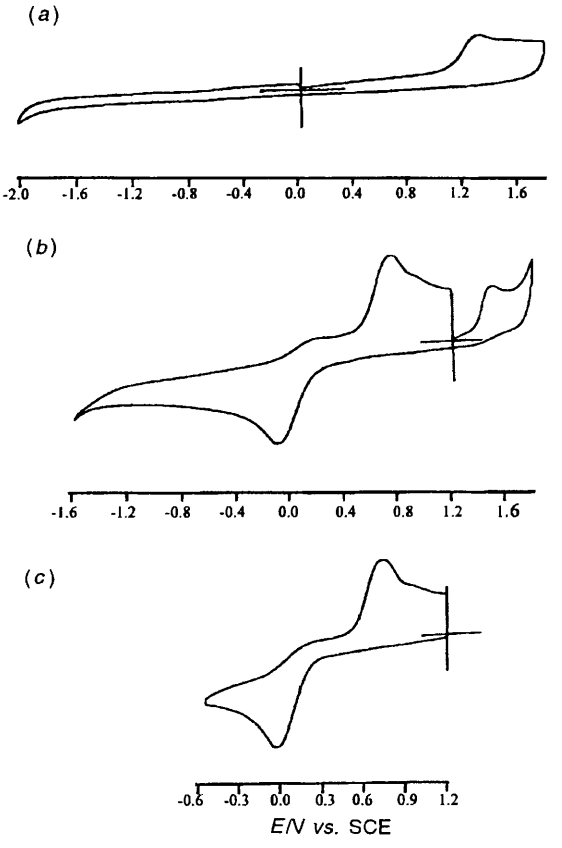

Fig. 6 Cyclic voltammagrams in CH_2Cl_2 containing $[NBu_4][BF_4]$ at 295 K of (*a*) compound L^1 in the scan range 0 to +1.8 and −2.0 to 0 V at a scan rate of 0.1 V s^{-1}, (*b*) $[CuL^1{}_2][BF_4]_2$ in the scan range +1.2 to +1.8 and to −1.6 to +1.2 at a scan rate of 0.2 V s^{-1} and (*c*) $[CuL^1{}_2][BF_4]_2$ in the scan range +1.2 to +0.6 and to −1.2 V at a scan rate of 0.2 V s^{-1}

Table 5 Reduction potentials, $E_{\frac{1}{2}}$ *vs.* SCE for Cu^{II}–Cu^{I} couples

Complex[a]	$E_{\frac{1}{2}}$/V	Ligand set	Solvent
$[CuL^6{}_2]^{2+/+}$	+0.59	N_4	MeCN
	+0.80		CH_2Cl_2
$[CuL^7{}_2]^{2+/+}$	+0.11	N_4	MeCN
$[CuL^8]^{2+/+}$	−0.35	N_5	MeCN
$[CuL^9]^{2+/+}$	−0.32	N_5	MeCN
$[CuL^{10}]^{2+/+}$	−0.20	N_5	MeCN
$[CuL^{11}]^{2+/+}$	+0.057	N_4	MeOH

[a] L^6 = Bis(1-methyl-4,5-diphenylimidazol-2-yl) ketone;[16] L^7 = 2,2′-bis(imidazol-2-yl)biphenyl;[31] L^8 = 2,6-bis{1-[2-(imidazol-4-yl)ethylimino]ethyl}pyridine;[32,33] L^9 = 2,6-bis{1-[2-(*N*-*p*-xylylimidazol-4-yl)-ethylimino]ethyl}pyridine;[32] L^{10} = 2,6-bis{1-[2-(pyridin-2-yl)ethylimino]ethyl}pyridine;[32,33] L^{11} = tetrabenzo[*b*,*f*,*j*,*n*][1,5,9,13]tetraazacyclohexadecine.[34,35]

back-bonding ability of imidazole ligands, and favourable overlap of the relevant π* (imidazole) orbitals with the metal HOMO d orbital. This would stabilise Cu^{I} with respect to Cu^{II}. This effect could be well developed for $[CuL^1{}_2]^{n+}$ given the geometry of the cation (Fig. 4) and the extensive π overlaps.

Conclusion

The five sterically hindered bis(imidazole) molecules, L^1–L^5 have been synthesised and characterised. These proligands show considerable variety in their tendency to co-ordinate to Cu^{II}. Important aspects are chelate 'bite' and the degree of steric hindrance presented to the metal. Compound L^1 reacts with $Cu(BF_4)_2{\cdot}4.5H_2O$ forming $[CuL^1{}_2][BF_4]_2$. The co-ordinating ability of this two-carbon bridge molecule can be explained in terms of the flexibility of the ethyl bridge which allows the substituted phenyl groups and the imidazole rings to orientate so that steric interactions between these groups have a small stabilisation which results from π-stacking of the rings.

The unreactivity of L^3 towards $Cu(BF_4)_2{\cdot}4.5H_2O$ can be rationalised on the basis of the steric hindrance of the imidazole relative to that of bpip. The steric interaction between the phenyl rings, the *trans*-adjacent co-ordinated imidazole, and the metal atom in any copper(II) complex presumably makes co-ordination of the metal unfavourable, with respect to the formation of the $[H_2L^3][BF_4]_2$ salt. Furthermore, the inflexibility of the one-carbon (methane) bridge excludes the possibility of the imidazole rings reorientating so as to reduce intramolecular steric interactions. Similar considerations are applicable to the unreactivity of L^2 with respect to complexation with $Cu(BF_4)_2{\cdot}4.5H_2O$.

The complexes $\{[CuL^5{}_2][BF_4]_2{\cdot}H_2O\}_n$ and $\{[CuL^4{}_2][BF_4]_2{\cdot}H_2O\}_n$ are polymeric, presumably due to the considerably larger bridge sizes of the xylyl-based groups linking the two imidazole rings plus the flexibility of these bridges.

Acknowledgements

We thank the SERC for a studentship to (T. C. H.) and funding provided by the EC Human Capital and Mobility Framework III MASIMO Network. J. McMaster, R. Bhalla, Drs. F. E. Mabbs and D. Collison are thanked for their valuable contributions.

References

1 J. M. Guss, E. A. Merritt, R. P. Phizackerley, B. Hedman, M. Murata, K. O. Hodgson and H. C. Freeman, *Science*, 1988, **241**, 806.
2 E. N. Baker, *J. Mol. Biol.*, 1988, **203**, 1071.
3 J. A. Tainer, E. D. Getzoff, K. M. Beem, J. S. Richardson and D. C. Richardson, *J. Mol. Biol.*, 1982, **160**, 181.
4 B. Linzen, N. M. Soeter, A. F. Riggs, H. J. Schneider, W. Schartau, M. D. Moore, E. Yokota, P. Q. Behrens, H. Nakashima, T. Takagi, J. M. Nemoto, J. M. Verijken, H. B. Bok, J. J. Beintena, A. Bolbeda, W. P. J. Gaykema and W. G. J. Hol, *Science*, 1985, **229**, 519.
5 N. Ito, S. E. V. Philips, C. Stevens, Z. B. Ogel, M. J. McPherson, J. N. Keen, K. D. S. Yadav and P. F. Knowles, *Nature* (*London*), 1991, **350**, 87.
6 A. Messerschmidt, A. Rossi, R. Ladenstein, R. Huber, M. Bolognesi, G. Gatti, A. Marchesini, R. Petruzelli and A. Finazzo-Agro, *J. Mol. Biol.*, 1989, **206**, 513.
7 J. W. Godden, S. Turley, D. C. Teller, E. T. Adman, M.-Y. Liu, W. J. Payne and J. LeGall, *Science*, 1991, **253**, 438.
8 D. L. McFadden, A. T. McPhail, P. M. Gross, C. D. Garner and F. E. Mabbs, *J. Chem. Soc., Dalton Trans.*, 1976, 47.
9 T. G. Fawcett, E. E. Bernarducci, K. Krogh-Jespersen and H. J. Schugar, *J. Am. Chem. Soc.*, 1980, **102**, 2598.
10 E. Bernarducci, J. L. Schwindinger, J. L. Hughey IV, K. Krogh-Jespersen and H. J. Schugar, *J. Am. Chem. Soc.*, 1981, **103**, 1686.
11 H. J. Schugar, *Copper Coordination Chemistry: Biochemical Inorganic Perspectives*, eds. K. D. Karlin and J. Zubieta, Adenine Press, New York, 1983, p. 43.
12 E. Bernarducci, P. K. Bharadwaj, K. Krogh-Jespersen, J. A. Potenza and H. J. Schugar, *J. Am. Chem. Soc.*, 1983, **105**, 3860.
13 E. Bernarducci, P. K. Bharadwaj, R. A. Lalancette, K. Krogh-Jespersen, J. A. Potenza and H. J. Schugar, *Inorg. Chem.*, 1983, **22**, 3911.
14 K. Krogh-Jespersen and H. J. Schugar, *Inorg. Chem.*, 1984, **23**, 4390.
15 T. C. Higgs, Ph.D. Thesis, University of Manchester, 1994.
16 J. McMaster, R. Beddoes, D. Collison, D. R. Eardley, M. Helliwell and C. D. Garner, *Chem. Eur. J.*, in the press.
17 R. Bhalla, personal communication.
18 H. J. Prochaska, W. F. Schwindinger, M. Schwartz, M. J. Burk, E. Bernarducci, R. A. Lalancette, J. A. Potenza and H. J. Schugar, *J. Am. Chem. Soc.*, 1981, **103**, 3446.
19 P. P. E. Strzybny, T. van Es and O. G. Backeberg, *J. Org. Chem.*, 1963, **28**, 3381.
20 N. Walker and D. Stuart, *Acta. Crystallogr., Sect. A*, 1983, **39**, 158.
21 C. J. Gilmore, MITHRIL: an Integrated Direct Methods Computer Program, University of Glasgow, *J. Appl. Crystallogr.*, 1984, **17**, 42.
22 P. T. Beurskens, DIRDIF: Direct Methods for Difference Structures – an automatic procedure for phase extension and refinement of difference structure factors, Technical Report 1984/1, Crystallographic Laboratory, Toernooiveld, Nijmegen, 1984.
23 G. M. Sheldrick, SHELXS 86, in *Crystallographic Computing 3*; eds. G. M. Sheldrick, C. Kreuger and R. Goddard, Oxford University Press, Oxford, 1985, p. 175.
24 D. T. Cromer and J. T. Waber, *International Tables for X-Ray Crystallography*, Kynoch Press, Birmingham, 1974, vol. 4.
25 C. K. Johnson, ORTEP, Report ORNL-5138, Oak Ridge National Laboratory, Oak Ridge, TN, 1976.
26 W. O. S. Motherwell and W. Clegg, PLUTO 78, University of Cambridge, 1978.
27 W. Vreugdenhil, P. J. M. W. L. Birker, R. W. N. ten Hoedt, G. C. Verschoor and J. Reedijk, *J. Chem. Soc., Dalton Trans.*, 1984, 429.
28 C. A. Hunter and J. K. M. Sanders, *J. Am. Chem. Soc.*, 1990, **112**, 5525.
29 F. E. Mabbs and D. Collison, *Electron Paramagnetic Resonance of d Transition Metal Compounds*; Elsevier, Amsterdam, 1992.
30 Southampton Electrochemistry Group; R. Greef, R. Peat, L. M. Peter, D. Fletcher and J. Robinson, *Instrumental Methods in Electrochemistry*; Ellis Horwood, Chichester, 1990.
31 S. Knapp, T. P. Keenan, X. Zhang, R. Fikar, J. A. Potenza and H. J. Schugar, *J. Am. Chem. Soc.*, 1990, **112**, 3452.
32 C. L. Merrill, L. J. Wilson, T. J. Thamann, T. M. Loehr, N. S. Ferris and W. H. Woodruff, *J. Chem. Soc., Dalton Trans.*, 1984, 2207.
33 J. A. Goodwin, D. M. Stanbury, L. J. Wilson, C. W. Eigenbrot and W. R. Scheidt, *J. Am. Chem. Soc.*, 1987, **109**, 2979.
34 N. E. Tokel, V. Katovic, K. Farmery, L. B. Anderson and D. H. Busch, *J. Am. Chem. Soc.*, 1970, **92**, 400.
35 E. J. Pulliam and D. R. McMillin, *Inorg. Chem.*, 1984, **23**, 1172.

Received 10*th October* 1995; *Paper* 5/06698K